Supporting information

Gram-scale Synthesis of Single-atom Metal-N-CNT Catalysts for Highly Efficient CO$_2$ Electroreduction

Qian Sun, Wenhao Ren, Yong Zhao and Chuan Zhao *

School of Chemistry, The University of New South Wales, Sydney, New South Wales 2052, Australia

* Corresponding author. E-mail: chuan.zhao@unsw.edu.au

SI Table of Contents

1. Experimental section

Chemicals

Nickel (II) acetate tetrahydrate, manganese (II) acetate tetrahydrate, iron (II) acetate, platinum (II) chloride, ruthenium (III) chloride, zinc (II) acetate dihydrate and carbon nanotube (multi-walled) were purchased from Sigma-Aldrich Pty Ltd. Cobalt (II) acetate tetrahydrate and dimethyl sulfoxide were purchased from Ajax Finechem Pty Ltd. Copper (II) acetate monohydrate and 1,10-Phenanthroline monohydrate were purchased from BDH Chemicals. Ethanol was purchased from Chem-Supply Pty. Ltd. All reagents and solvents were of analytical grade and used as received without additional purification. The CO_2 and Ar feed gases were purchased from air liquide in Australia.

Preparation of Ni-N-CNT

In a typical experiment of preparing 1.5 % Ni-N-CNT (1.5 wt%), multiwalled carbon nanotube (76.44 mg) was dispersed in ethanol (4 mL) with ultrasonication for 2 h to get a uniform suspension solution. At the same time, 1, 10-phenonathroline monohydrate (14.85 mg) and nickel acetate tetrahydrate (6.20 mg) (molar ratio of 3:1 for 1,10-phenanthroline: Ni) were dissolved in ethanol (2 mL) under stirring at room temperature. This solution was then added into the carbon nanotube suspension to get a mixed solution. After which, the mixed solution was heated at 60 °C for 4 h in oil-bath with stirring and then at 80 °C for 2 h to evaporate ethanol, yielding a black solid. After cooling down to room temperature, the black solid was lightly ground using a mortar and pestle, then transferred into a ceramic crucible and put in a tube furnace. The black solid was heated at 350 °C for 2 h and then 1000 °C for 2 h at a ramping rate of 5 °C/min under Ar flow, the final product was obtained and denoted as 1.5 % Ni-N-CNT. Using similar methods, x % Ni-N-CNT (x=1, 2, 2.5, 3, 3.5) was prepared.

Large-scale synthesis of Ni-N-CNT

Large-scale synthesis of Ni-N-CNT was carried out using the same procedures as for 1.5 % Ni-N-CNT but with different mass of the reactants: multiwalled carbon nanotube (1528.8 mg), 1, 10-phenonathroline monohydrate (297 mg), nickel acetate tetrahydrate (124 mg). The obtained final product Ni-N-CNT with 1.5 wt% Ni loading was 1535.2 mg with high yield of 78.74 % (the yield was calculated as the ratio of the mass of final product Ni-N-CNT to the total mass of multiwalled carbon nanotube, 1, 10-phenonathroline monohydrate, and nickel acetate tetrahydrate), which confirmed the mass-production of Ni-N-CNT.

Preparation of CNT-N, CNT-Ni, and CNT

CNT-N and CNT-Ni were prepared using same steps for 1.5 % Ni-N-CNT but

without introducing nickel acetate tetrahydrate and 1, 10-phenonathroline monohydrate. CNT was heated at 350 °C for 2 h and then 1000 °C for 2 h at a ramping rate of 5 °C/min under Ar flow.

Preparation of 1.5 % Mn-N-CNT, 1.5 % Fe-N-CNT, 1.5 % Co-N-CNT and 1.5 % Zn-N-CNT

Different metal salts (manganese (II) acetate tetrahydrate, iron (II) acetate, cobalt (II) acetate tetrahydrate and zinc (II) acetate dihydrate) and 1,10-phenanthroline monohydrate were used. Keep the molar ratio of 1,10-phenanthroline: metal be 3:1. Preparation procedures were the same as that for 1.5% Ni-N-CNT.

Preparation of 1.5 % Cu-N-CNT, 1.5 % Ru-N-CNT and 1.5 % Pt-N-CNT

Metal precursors copper (II) acetate monohydrate, ruthenium (III) chloride and platinum (II) chloride, and nitrogen precursor 1,10-phenanthroline monohydrate were employed to prepare these catalysts. Synthetic steps were same as that for 1.5% Ni-N-CNT, except that DMSO rather than ethanol was used. Because of higher boiling point of DMSO, the solvent was evaporated at 190 °C.

Catalyst characterizations

The details of structure and morphology of the fabricated materials were investigated X-ray diffractometer (Rigaku MiniFlex), X-ray photoelectron spectroscopy (Thermo Scientific ESCALAB 250Xi), ICP-OES and scanning electron microscope (SEM, JSM-7001F, and QUANTA 450). Aberration-corrected high-angle annular dark-field scanning transmission electron microscopy (HAADF-STEM) and Energy-dispersive X-ray spectroscopy (EDS) were obtained from JEOL JEM-ARM200F.

Electrochemical measurements

A three-electrode sealed H-type cell was employed for all electrochemical tests. Catalysts (5 mg) were introduced in a solution of H_2O (150 μL), ethanol (50 μL), and 5 wt% Nafion solution (50 μL). After sonication for 2 h, a uniform catalyst ink was obtained. Then, the ink was dropped onto a polished glassy carbon and dried in air, giving a working electrode with catalyst loading of 0.5-1 mg cm^{-2}. The reference and counter electrodes were a saturated calomel electrode (SCE) electrode and a Pt wire. All LSV and potentiostatic data were collected in 0.5 M $KHCO_3$ and corrected with 90 % IR compensation. All potentials were calculated using the Nernst equation:

$E_{RHE} = E_{SCE} + 0.0591 \times pH + 0.241$ V (25 °C)

The products and Faradic efficiency of CO_2 electroreduction were measured by chronoamperometry at fixed potentials. The gaseous products were quantified by a gas chromatograph with a flame ionization detector (FID) for CO and CH_4 and a

thermal conductivity detector for H_2 quantification. The carrier gas was ultrapure Ar (99.999%). The CO_2 flow rate was 20 sccm controlled by a Cole-Parmer mass flow meter.

The faradaic efficiencies were calculated as the following:

$$FE_{CO} = \frac{0.1315 \times V_{CO2} \times \left(\dfrac{0.015039A_{CO}}{1000000}\right)}{I_{total}} \times 100\%$$

$$FE_{H2} = \frac{0.1315 \times V_{CO2} \times \left(\dfrac{10.87417A_{H2} - 36.35039}{1000000}\right)}{I_{total}} \times 100\%$$

V_{CO2}: flow rate (sccm)

A_{CO}: integral area of CO peak tested by GC

A_{H2}: integral area of H_2 peak tested by GC

I_{total}: total current (A)

Electrochemical active surface areas (ECSA) measurements

The ECSA is proportional to double-layer capacitance (C_{dl}) values. C_{dl} was determined in H-type cell by measuring the capacitive current associated with double-layer charging from the scan-rate dependence of cyclic voltammetry (CV). The CV ranged from -0.5 to -0.6 V vs SCE. The scan rates were 10, 20, 40, 60, 80 and 100 mV/s. C_{dl} was estimated by plotting the anodic and cathodic current density difference at -0.55 V vs SCE against the scan rates.

ECSA was calculated based on the definition:

ECSA = C_{dl}/C_s

Where C_{dl} corresponds to the slope of the double-layer charging current vs the scan rate plot, and the value of C_s we used is 40 µF cm^{-2}.
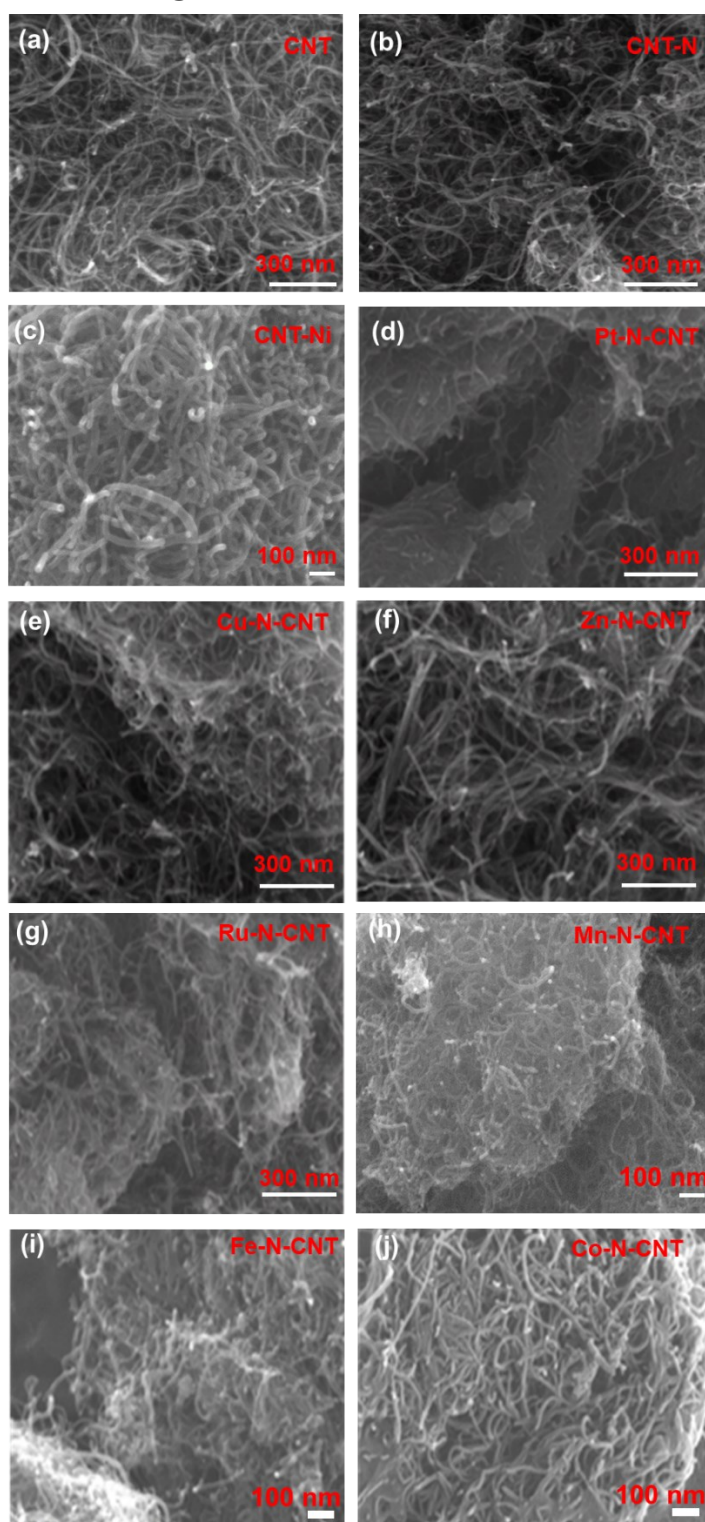
2. Supplemental Figures

Fig. S1 SEM images of (a) CNT, (b) CNT–N, (c) CNT-Ni, (d) Pt-N-CNT, (e) Cu-N-CNT, (f) Zn-N-CNT, (g) Ru-N-CNT, (h) Mn-N-CNT, (i) Fe-N-CNT, (j) Co-N-CNT.
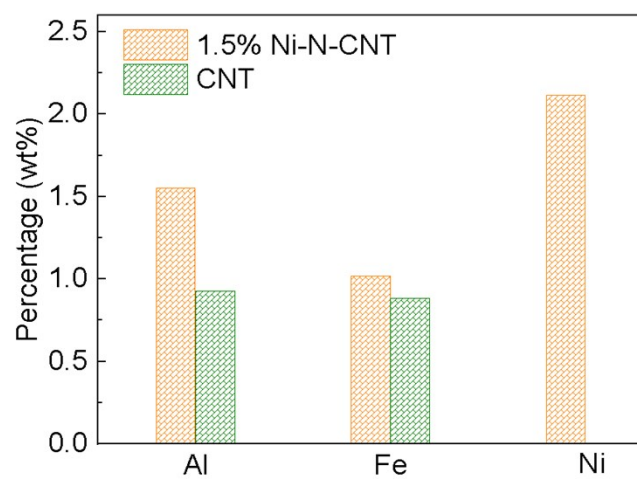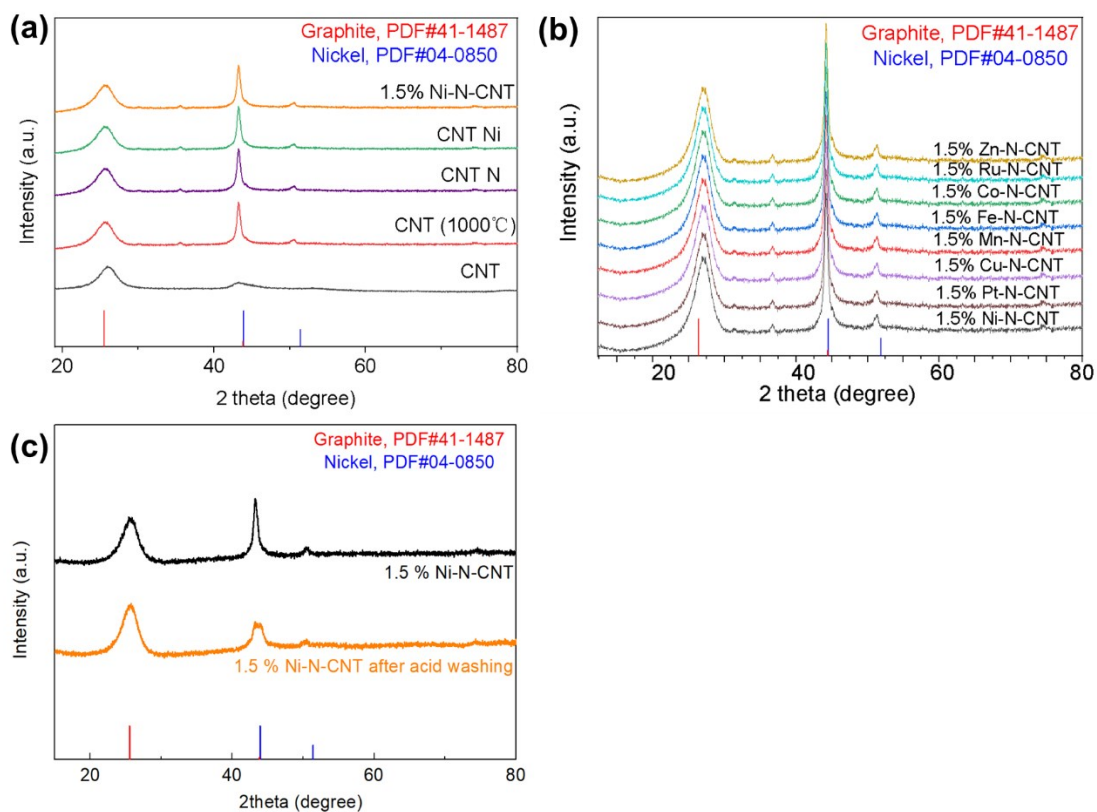
Fig. S2 ICP data for 1.5% Ni-N-CNT and CNT.

Fig. S3 X-ray diffraction patterns of (a) 1.5% Ni-N-CNT and reference catalysts, (b) different metal single atom catalyst, and (c) 1.5 % Ni-N-CNT after acid washing with 3M HCl at room temperature for 8h.
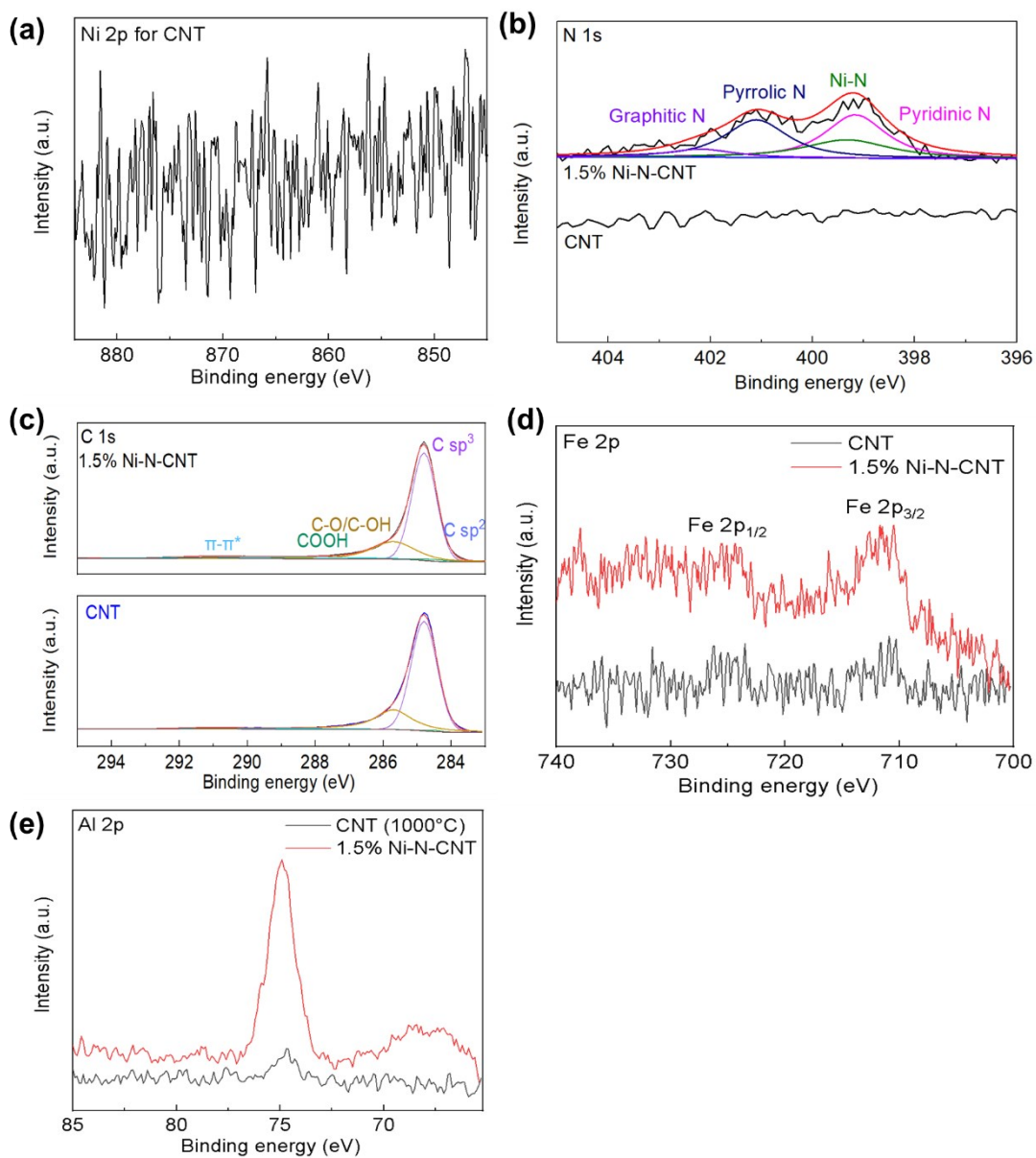
Fig. S4 X-ray spectroscopy of (a) Ni 2p XPS spectrum of CNT, (b) N 1s XPS spectrum, (c) C 1s XPS spectrum, (d) Fe 2p XPS spectrum and (e) Al 2p XPS spectrum of 1.5% Ni-N-CNT and CNT.
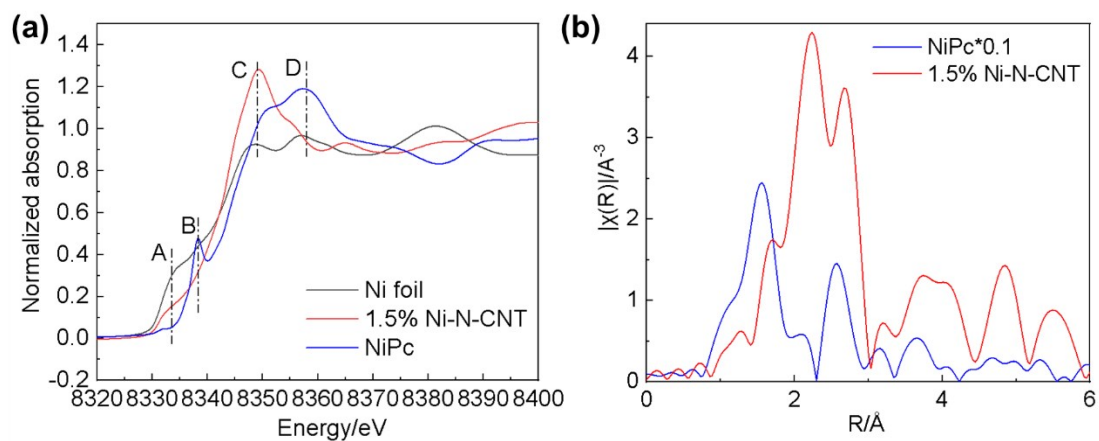
Fig. S5 (a) Ni K-edge XANES spectra of Ni foil, NiPc, and 1.5%Ni-N-CNT. (b) Fourier transformation of the EXAFS spectra at R space.
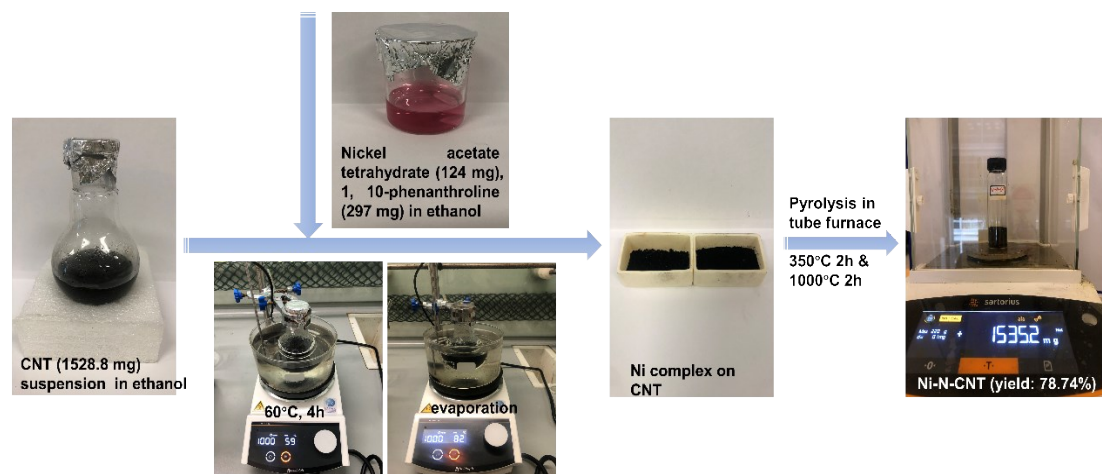
Fig. S6 Synthetic route for preparing Ni-N-CNT at large-scale.
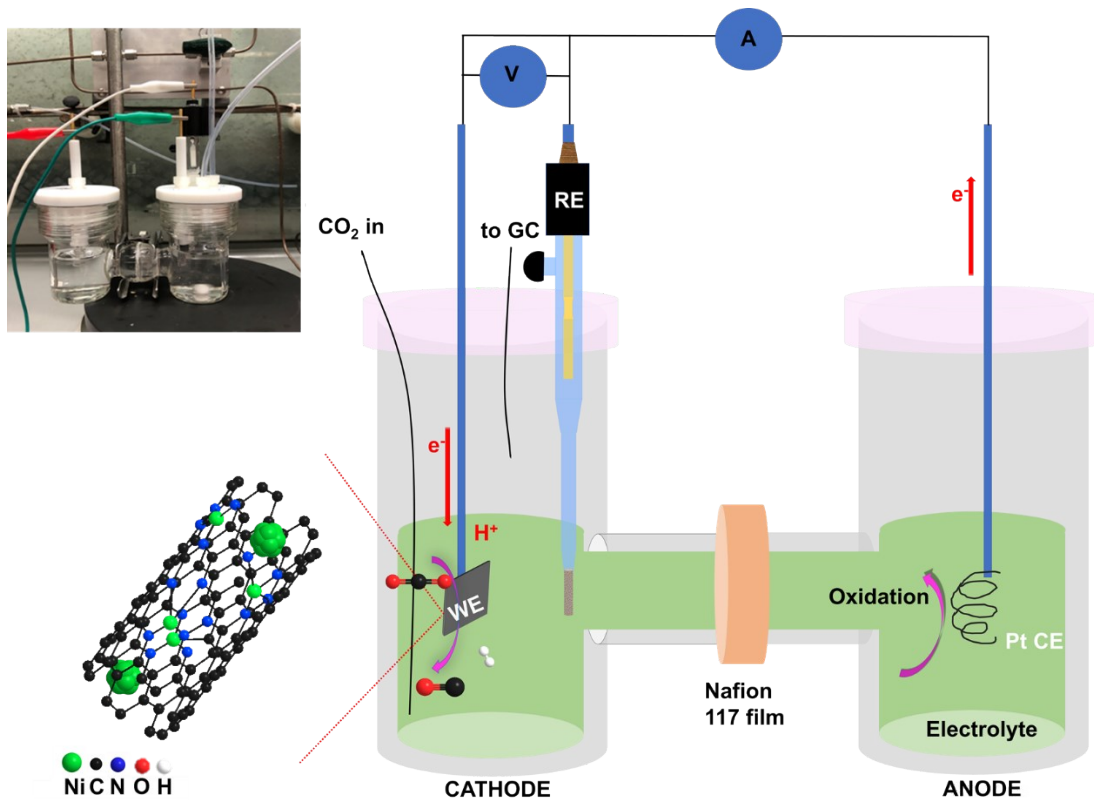
Fig. S7 Schematic of CO_2 electrolysis in H-cell.

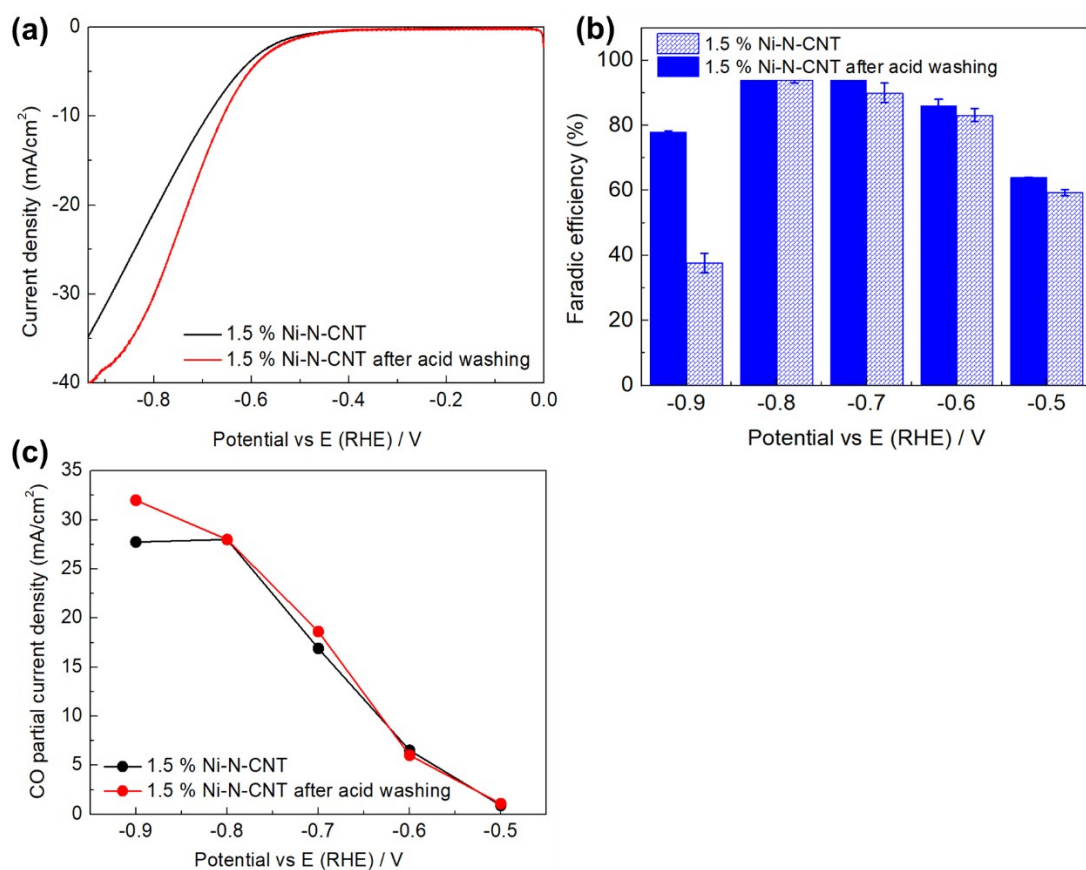**Fig. S8** (a) LSV, (b) FE$_{CO}$, and (c) CO partial current density of 1.5 % Ni-N-CNT and 1.5 % Ni-N-CNT after acid washing with 3M HCl at room temperature for 8h.
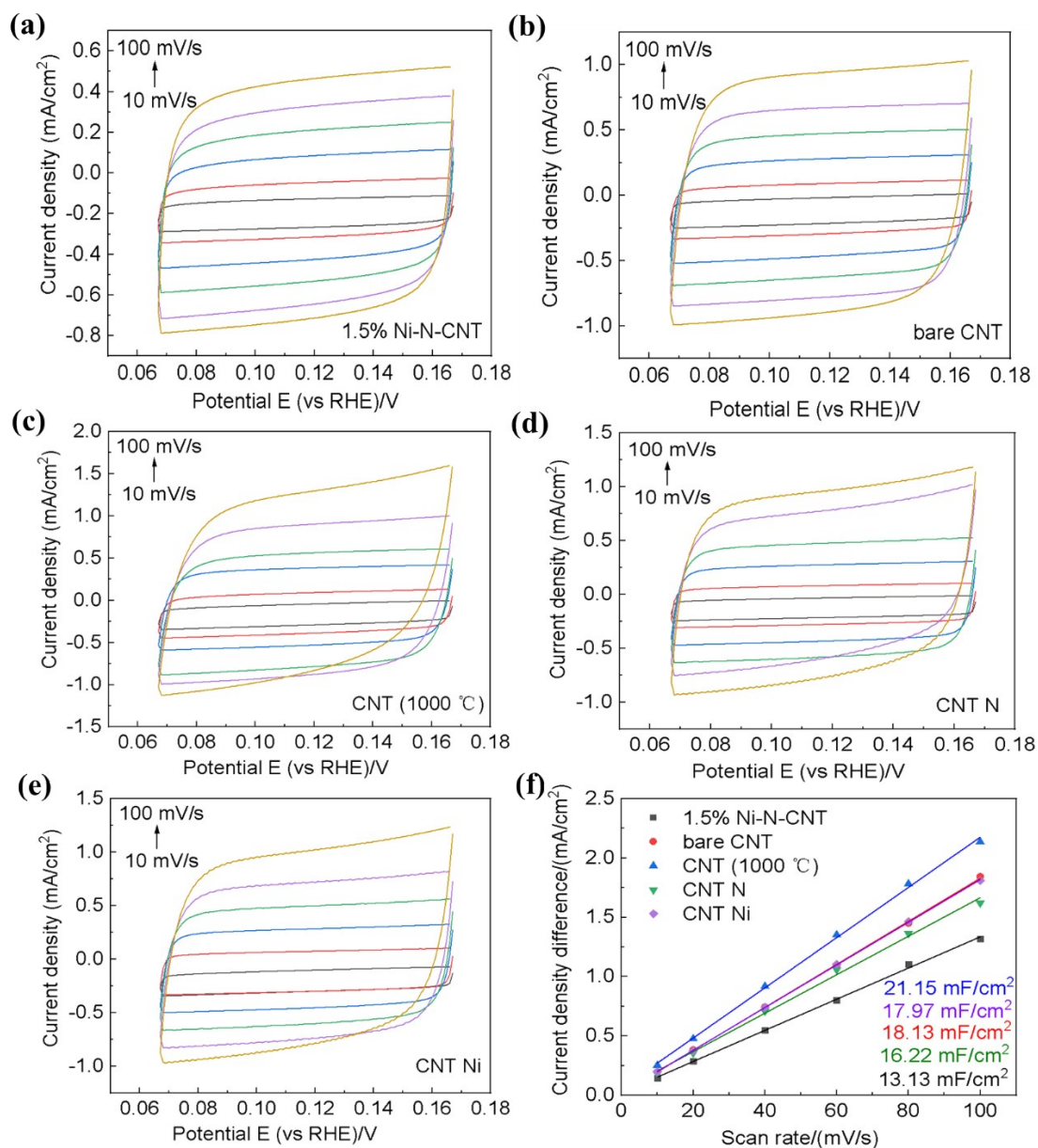
Fig. S9 CVs of (a) 1.5% Ni-N-CNT, (b) bare CNT, (c) CNT, (d) CNT N, and (e) CNT Ni with various scan rates (10-100 mV/s) in the region of 0.067 to 0.167 V vs. RHE. (f) Charging current density differences plotted against scan rates for these samples.

Fig. S10 CVs of (a) 1.5% Co-N-CNT, (b) 1.5% Cu-N-CNT, (c) 1.5% Fe-N-CNT, (d) 1.5% Mn-N-CNT, (e) 1.5% Pt-N-CNT, (f) 1.5% Ru-N-CNT, and (g) 1.5% Zn-N-CNT with various scan rates (10-100 mV/s) in the region of 0.067 to 0.167 V vs. RHE. (h) Charging current density differences plotted against scan rates for these samples.
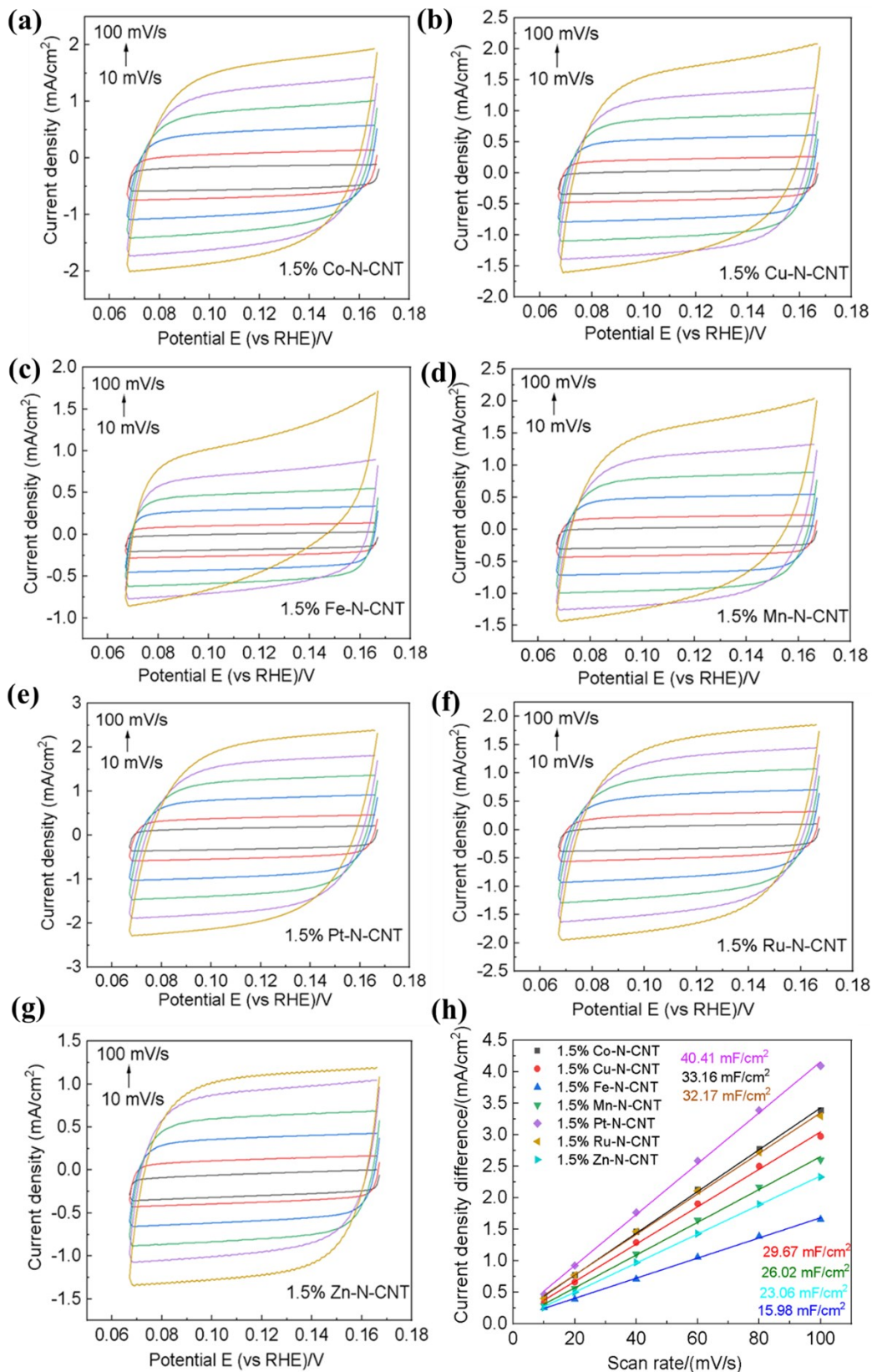
3. Table

Table S1 Comparison of different catalysts for the CO_2RR performance towards CO

Materials	Electrolyte	Cell	E/V vs. RHE	FE/%	J/mA cm^{-2}	Ref.
Ni-N-CNT	0.5 M KHCO$_3$	H-cell	-0.8	94	28	This work
Ni-N-C	0.5 M KHCO$_3$	H-cell	-0.9	71.9	10.48	[1]
Ni-N-CNT	0.5 M KHCO$_3$	H-cell	-0.7	91.3	23.5	[2]
Ni-N-MEGO	0.5 M KHCO$_3$	H-cell	-0.7	92.1	26.8	[3]
Ni-N-Graphene	0.5 M KHCO$_3$	H-cell	-0.68	92	10.2	[4]
Ni-N-Gr	0.1 M KHCO$_3$	H-cell	-0.8	90	-	[5]
Ni-NG	0.5 M KHCO$_3$	H-cell	-0.62	95	$\sim$11	[6]
A-Ni-NSG	0.5 M KHCO$_3$	H-cell	-0.8	$\sim$90	22.5 mA cm^{-2} @ -0.72 V	[7]
A-Ni-NG	0.5 M KHCO$_3$	H-cell	-0.8	$\sim$90	-	[7]
NC-CNTs	0.1 M KHCO$_3$	H-cell	-0.8	$\sim$90	-	[8]
Ni-CNT-CONH	0.5 M KHCO$_3$	H-cell	-0.65	98	18.6	[9]
Ni-CNT-PP	0.5 M KHCO$_3$	H-cell	-0.65	96	13.4	[9]
Ni-N-RGO	0.5 M KHCO$_3$	H-cell	-0.8	97	5 mA cm^{-2} @ -0.71 V	[10]
Ni-N-C	0.1 M KHCO$_3$	H-cell	-0.78	85	-	[11]
NiSA-NGA	0.5 M KHCO$_3$	H-cell	-0.8	90.2	-	[12]
NiN-GS	0.1 M KHCO$_3$	H-cell	-0.8	93	-	[13]
SANi-GO	0.5 M KHCO$_3$	H-cell	-0.63	96.5	8.3	[14]
Ni/NC	0.1 M KHCO$_3$	H-cell	-0.9	96.5	12.6 mA cm^{-2} @ -1.2 V	[15]
Ni/NC	0.1 M KHCO$_3$	H-cell	-0.8	92.3	4	[16]
Ni SAC	0.5 M KHCO$_3$	H-cell	-0.65	95.2	>15	[17]
Ni$_{IMP}$/NC$_{923}$	0.1 M KHCO$_3$	H-cell	-0.6	82	-	[18]

4. References

1. C. M. Zhao, X. Y. Dai, T. Yao, W. X. Chen, X. Q. Wang, J. Wang, J. Yang, S. Q. Wei, Y. Wu and Y. D. Li, *J. Am. Chem. Soc.*, 2017, **139**, 8078.

2. Y. Cheng, S. Y. Zhao, B. Johannessen, J. P. Veder, M. Saunders, M. R. Rowles, M. Cheng, C. Liu, M. F. Chisholm, R. D. Marco and H. M. Cheng, *Adv. Mater.*, 2018, **30**, 1706287.

3. Y. Cheng, S. Y. Zhao, H. B. Li, S. He, J. P. Veder, B. Johannessen, J. P. Xiao, S. F. Lu, J. Pan, M. F. Chisholm, S. Z. Yang, C. Liu, J. G.Chen and S. P. Jiang, *Appl. Catal. B*, 2019, **243**, 294.

4. W. T. Bi, X. G. Li, R. You, M. L. Chen, R. L. Yuan, W. X. Huang, X. J. Wu, W. S. Chu, C. Z. Wu and Y. Xie, *Adv. Mater.*, 2018, **30**, 1706617.

5. P. P. Su, K. Iwase, S. Nakanishi, K. Hashimoto and K. Kamiya, *Small*, 2016, **12**, 6083.

6. K. Jiang, S. Siahrostami, T. T. Zheng, Y. F. Hu, S. Hwang, E. Stavitski, Y. Peng, J. Dynes, M. Gangisetty, D. Su, K. Attenkofer and H. T. Wang, *Energy Environ. Sci.*, 2018, **11**, 893.

7. H. B. Yang, S. F. Hung, S. Liu, K. D. Yuan, S. Miao, L. P. Zhang, X. Huang, H. Y. Wang, W. Z. Cai, R. Chen, J. J. Gao, X. F. Yang, W. Chen, Y. Q. Huang, H. M. Chen, C. M. Li, T. Zhang and B. Liu, *Nat. Energy*, 2018, **3**, 140.

8. Q. Fan, P. F. Hou, C. Choi, T. S. Wu, S. Hong, F. Li, Y. L. Soo, P. Kang, Y. Jung, Z. Sun, *Adv. Energy Mater.*, 2019, 1903068.

9. S. Liu, H. B. Yang, S. F. Hung, J. Ding, W. Cai, L. Liu and Y. Huang, *Angew. Chem. Int. Ed.*, 2019, **59**, 798.

10. H. Y. Jeong, M. Balamurugan, V. S. K. Choutipalli, J. Jo, H. Baik, V. Subramanian, M. Kim, U. Sim and K. T. Nam, *Chem. Eur. J*, 2018, **24**, 18444.

11. W. Ju, A. Bagger, G. P. Hao, A. S. Varela, I. Sinev, V. Bon, B. R. Cuenya, S. Kaskel, J. Rossmeisl and P. Strasser, *Nat. Commun.*, 2017, **8**, 1.

12. K. W. Mou, Z. P. Chen, X. X. Zhang, M. Y. Jiao, X. P. Zhang, X. Ge, W. Zhang, L. C. Liu, *Small*, 2019, **15**, 1903668.

13. K. Jiang, G. X. Chen and H. T. Wang, *J. Vis. Exp.*, 2018, **134**, e57380.

14. S. Y. Zhao, G. X. Chen, G. M. Zhou, L. C. Yin, J. P. Veder, B. Johannessen, M. Saunders, S. Z. Yang,   R. D. Marco, C. Liu and S. P. Jiang, *Adv. Funct. Mater.*, 2019, **30**, 1906157.

15. M. L. Zhang, T. S. Wu, S. Hong, Q. Fan, Y. L. Soo, J. Masa, J. S. Qiu and Z. Y. Sun, A*CS Sustain. Chem. Eng.*, 2019, **7**, 15030.

16. F. Li, S. Hong, T. S. Wu, X. Li, J. Masa, Y. L. Soo and Z. Y. Sun, *ACS Appl. Energy Mater.*, 2019, **2**, 8836.

17. W. L. Zhu, J. J. Fu, J. Liu, Y. Chen, X. Li, K. K. Huang, Y. M. Cai, Y. M. He, Y. Zhou, D. Su, J. J. Zhu and Y. H. Lin, *Appl. Catal. B*, 2020, **264**, 118502.

18. S. Büchele, A. J. Martín, S. Mitchell, F. Krumeich, S. M. Collins, S. Xi, A. Borgna and J. P. Ramírez, *ACS Catal.*, 2020, **10**, 3444.